Chemistry of Gold in Molten Alkali Metal Polychalcophosphate Fluxes. Synthesis and Characterization of the Low-Dimensional Compounds $A_3AuP_2Se_8$ (A = K, Rb, Cs), $A_2Au_2P_2Se_6$ (A = K, Rb), A_2AuPS_4 (A = K, Rb, Cs), and $AAuP_2S_7$ (A = K, Rb)

Konstantinos Chondroudis, Jason A. Hanko, and Mercouri G. Kanatzidis*

Department of Chemistry, Michigan State University, East Lansing, Michigan 48824

Received November 18, 1996[⊗]

The reaction of Au with a molten mixture of $A_2Q/P_2Q_5/Q$ (Q = S, Se) produced the quaternary compounds $A_3AuP_2Se_8$ (A = K, Rb, Cs) (**I**−**III**), $A_2Au_2P_2Se_6$ (A = K, Rb) (**IV**, **V**), A_2AuPS_4 (A = K, Rb, Cs) (**VI**−**VIII**), and $AAuP_2S_7$ (A = K, Rb) (**IX**, **X**). **I**−**III** crystallize in the acentric space group *Cc* (No. 9): **I**, $a = 7.122(2)$ Å, $b = 12.527(3)$ Å, $c = 18.666(4)$ Å, $\beta = 96.06(2)°$, $Z = 4$. **IV** and **V** crystallize in the space group *C*2/*m* (No. 12): **IV**, $a = 12.289(2)$ Å, $b = 7.210(1)$ Å, $c = 8.107(1)$ Å, $\beta = 115.13(1)°$, $Z = 2$. **VI** and **VII** crystallize in the space group $P2_1/m$ (No. 11): **VI**, $a = 6.518(2)$ Å, $b = 6.747(2)$ Å, $c = 9.468(3)$ Å, $\beta = 92.98(2)°$, $Z = 2$. **VIII** crystallizes in the space group *Pbcm* (No. 57) with $a = 6.904(3)$ Å, $b = 20.093(6)$ Å, $c = 7.025(5)$ Å, and $Z = 4$. **IX** and **X** crystallize in the space group *C*2/*c* (No. 15): **IX**, $a = 7.917(3)$ Å, $b = 9.247(2)$ Å, $c = 14.968(3)$ Å, $\beta = 91.84(9)°$, $Z = 4$. Compounds **I**−**III** have a one-dimensional structure with $[AuP_2Se_8]_n^{3n-}$ chains separated by A^+ cations. The monovalent Au cation is linearly coordinated to the new ligand $[P_2Se_8]^{4-}$. **IV** and **V** possess a one-dimensional structure with $[Au_2P_2Se_6]_n^{2n-}$ chains separated by A^+ ions. The monovalent Au cation is linearly coordinated to ethane like $[P_2Se_6]^{4-}$ ligands. **VI** and **VII** have a one-dimensional structure with $[AuPS_4]_n^{2n-}$ chains separated by A^+ cations. The Au^+ cation is linearly coordinated to alternating $[PS_4]^{3-}$ tetrahedra. The structure of **VIII** is related to that of **I**−**III** with $[AuPS_4]_n^{2n-}$ chains. The diselenide of the $[P_2Se_8]^{4-}$ unit is replaced by a second, essentially linear, S−Au−S linkage leaving the structure of the chain unchanged. **IX** and **X** have the $[AuP_2S_7]^{n-}$ chains with square planar Au^{3+} centers. The compounds were characterized with differential thermal analysis, far-IR, Raman spectroscopy, solid-state UV/vis diffuse reflectance spectroscopy, and single-crystal optical spectroscopy. Cs_2AuPS_4, at $T > 375$ °C, converts to β-Cs_2AuPS_4, which is isostructural to K_2AuPS_4.

1. Introduction

The polychalcophosphate fluxes provide the best set of experimental conditions for the synthesis of new ternary and quaternary thiophosphate and selenophosphate compounds.[1] These fluxes form by the *in situ* fusion of $A_2Q/P_2Q_5/Q$ and contain $[P_yQ_z]^{n-}$ (Q = S, Se) units which, in the presence of metal ions, coordinate to give interesting new materials. These materials tend to be structurally and compositionally complex and often cannot be made by standard solid-state chemistry methods. After the initial report on $ABiP_2S_7$ (A = K, Rb),[2] the following unusual compounds were reported: $A_3M(PS_4)_2$ (A = Rb, Cs; M = Sb, Bi),[3] $Cs_3Bi_2(PS_4)_3$,[3] $Na_{0.16}Bi_{1.28}P_2S_6$,[3] $A_2MP_2Se_6$ (A = K, Rb; M = Mn, Fe),[1] $A_2M_2P_2Se_6$ (A = K, Cs; M = Cu, Ag),[1] KMP_2Se_6 (M = Sb, Bi),[4] $Cs_8M_4(P_2Se_6)_5$ (M = Sb, Bi),[5] $APbPSe_4$,[6] $A_4M(PSe_4)_2$ (A = Rb, Cs; M = Pb, Eu),[6] $Rb_4Ti_2(P_2Se_9)_2(P_2Se_7)$,[7] $KTiPSe_5$,[7] $A_5Sn(PSe_5)_3$ (A = K, Rb),[8] $A_6Sn_2Se_4(PSe_5)_2$ (A = Rb, Cs),[8a] and $Rb_8M_4(Se_2)_2(PSe_4)_4$[8b] (M = Cd, Hg). More recently, $K_2UP_3Se_9$,[9a] $Rb_4U_4P_4Se_{26}$,[9b] and the $K(RE)P_2Se_6$ (RE = Y, La, Ce, Pr, Gd)[10] series were also reported. Extension of this chemistry to Au looked appealing because no structurally characterized compounds have been reported. The only reported compound is the ternary $AuPS_4$,[11] whose structure remains elusive. On the basis of vibrational spectroscopy, a polymeric chain structure consisting of alternating edge-sharing PS_4 tetrahedra and square AuS_4 planes was proposed. Our studies with Au yielded the first structurally characterized gold selenophosphate compound, the mixed-valent $A_6Au^{I}_{1.5}Au^{III}_{1.5}(P_2Se_6)_3$ (A = K, Rb)[12] which features three-coordination geometries for the Au centers.

Here we report the synthesis, structural characterization, and optical and thermal properties of the new quaternary gold selenophosphate compounds $A_3AuP_2Se_8$ (A = K, Rb, and Cs) and $A_2Au_2P_2Se_6$ (A = K and Rb). The thiophosphate chemistry was also studied in order to investigate the existence of isostructural compounds and to synthesize new structural types.

[⊗] Abstract published in *Advance ACS Abstracts*, May 15, 1997.

(1) (a) McCarthy, T. J.; Kanatzidis, M. G. *Inorg. Chem.* **1995**, *34*, 1257−1267 and references therein. (b) Sutorik, A.; Kanatzidis, M. G. *Prog. Inorg. Chem.* **1995**, *43*, 151−265.
(2) McCarthy, T. J.; Hogan, T.; Kannewurf, C. R.; Kanatzidis, M. G. *Chem. Mater.* **1994**, *6*, 1072−1079.
(3) McCarthy, T. J.; Kanatzidis, M. G. *J. Alloys Comp.* **1996**, *236*, 70−85.
(4) McCarthy, T. J.; Kanatzidis, M. G. *J. Chem. Soc., Chem. Commun.* **1994**, 1089−1090.
(5) McCarthy, T. J.; Kanatzidis,M. G. *Chem. Mater.* **1993**, *5*, 1061−1063.
(6) Chondroudis, K.; McCarthy, T. J.; Kanatzidis, M. G. *Inorg. Chem.* **1996**, *35*, 840−844.
(7) Chondroudis, K.; Kanatzidis, M. G. *Inorg. Chem.* **1995**, *34*, 5401−5402.
(8) (a) Chondroudis, K.; Kanatzidis, M. G. *J. Chem. Soc., Chem. Commun.* **1996**, 1371−1372. (b) Chondroudis, K.; Kanatzidis, M. G. *J. Chem. Soc., Chem. Commun.* **1997**, 401−402.
(9) (a) Chondroudis, K.; Kanatzidis, M. G. *C. R. Acad. Sci. Paris, Ser. B* **1996**, *322*, 887−894. (b) Chondroudis, K.; Kanatzidis, M. G. *J. Am. Chem. Soc.* **1997**, *119*, 2574−2575.
(10) (a) Chen, J. H.; Dorhout, P. K. *Inorg. Chem.* **1995**, *34*, 5705−5706. (b) Chen, J. H.; Dorhout, P. K. Ostenson, J. E. *Inorg. Chem.* **1996**, *35*, 5627−5633.
(11) Pätzmann, U.; Brockner, W.; Cyvin, B. N.; Cyvin, S. *J. Raman Spectrosc.* **1986**, *17*, 257−261.
(12) Chondroudis, K.; McCarthy, T. J.; Kanatzidis, M. G. *Inorg. Chem.* **1996**, *35*, 3451−3452.

S0020-1669(96)01376-6 CCC: $14.00

These studies led to two additional types of gold thiophosphates, A_2AuPS_4 (A = K, Rb, and Cs) and $AAuP_2S_7$ (A = K, Rb), which represent the first structurally characterized examples of quaternary gold thiophosphates. Access to each phase was achieved with modifying the flux basicity, by means of varying the amount of A_2Q and P_2Q_5 in the starting composition (see Syntheses).[1,6−9,12]

2. Experimental Section

2.1. Reagents. The reagents mentioned in this study were used as obtained as follows unless noted otherwise: (i) Au metal (99.99%), Liberty Coins, Lansing MI; (ii) phosphorus pentasulfide (P_2S_5) 99.999% purity, Aldrich Chemical Co., Milwaukee, WI; (iii) red phosphorus powder, −100 mesh, Morton Thiokol, Inc., Danvers, MA. (iv) cesium metal, analytical reagent, Johnson Matthey/AESAR Group, Seabrook, NH; (v) rubidum metal, analytical reagent, Johnson Matthey/AESAR Group, Seabrook, NH; (vi) potassium metal, analytical reagent, Aldrich Chemical Co., Milwaukee, WI; (vii) sulfur powder, sublimed, J. T. Baker Chemical Co., Phillipsburg, NJ; (viii) selenium powder, 99.5+% purity, −100 mesh, Aldrich Chemical Co., Inc., Milwaukee, WI; (ix) *N*,*N*-dimethylformalide (DMF) reagent grade, EM Science, Inc., Gibbstown, NJ; (x) diethyl ether, ACS anhydrous, EM Science, Inc., Gibbstown, NJ; (xi) methanol (MeOH) ACS anhydrous, EM Science, Inc., Gibbstown, NJ.

Finely Divided Au Metal. A Canadian maple leaf gold coin, (99.99%, 31.1g) was dissolved in 400 mL of *aqua regia* (300 mL of concentrated HCl and 100 mL of concentrated HNO_3). The solution was boiled in an acid-resistant fume hood to a volume of approximately 100 mL. The solution was neutralized with ammonium hydroxide, and the gold was reduced with excess hydrazine hydrochloride, dissolved in 100 mL of distilled water. The resulting black suspension was gently heated, with stirring, for 1 h to allow particle aggregation. After the suspension was filtered and washed with copious amounts of distilled water and acetone, the resulting gold powder was heated in air for 2 h at 200 °C to drive off any remaining impurities, yielding 30.9 g of Au powder. *Note*: Heating too long or at higher temperature results in impractical grain sizes.

2.2. Syntheses. A_2Q (A = K, Rb, Cs; Q = S, Se) compounds were prepared by reacting stoichiometric amounts of the elements in liquid ammonia as described elsewhere.[1a,2]

P_2Se_5. The amorphous phosphorus selenide glass "P_2Se_5" was prepared by heating a stoichiometric ratio of the elements as described elsewhere.[1]

Preparation of $K_3AuP_2Se_8$ (I). A mixture of Au (0.3 mmol), P_2Se_5 (0.6 mmol), K_2Se (1.2 mmol), and Se (3.0 mmol) was sealed under vacuum in a Pyrex tube and heated to 440 °C for 4 d followed by cooling to 150 °C at 4 °C h^{-1}. The excess $A_x[P_ySe_z]$ flux was removed by washing with DMF to reveal analytically pure orange-yellow plates (87% yield based on Au). The crystals are only stable for some days in air and water. Microprobe analysis carried out on several randomly selected crystals gave an average composition of $K_{2.9}AuP_{1.8}Se_{8.1}$.

Preparation of $Rb_3AuP_2Se_8$ (II). A mixture of Au (0.3 mmol), P_2Se_5 (0.6 mmol), Rb_2Se (1.2 mmol), and Se (3.0 mmol) was sealed under vacuum in a Pyrex tube and heated as in **I**. The flux was removed as in **I** to reveal analytically pure orange-yellow plates (84% yield based on Au). The crystals are only stable for some days in air and water. Microprobe analysis gave an average composition of $Rb_{2.8}AuP_{1.9}Se_{7.9}$.

Preparation of $Cs_3AuP_2Se_8$ (III). A mixture of Au (0.3 mmol), P_2Se_5 (0.6 mmol), Cs_2Se (1.2 mmol), and Se (3.0 mmol) was sealed under vacuum in a Pyrex tube and heated as in **I**. The flux was removed as in **I** to reveal analytically pure orange-yellow plates (81% yield based on Au). The crystals are stable in air and water (signs of decomposition are apparent only after several weeks). Microprobe analysis gave an average composition of $Cs_{2.7}AuP_{2.0}Se_{8.0}$.

Preparation of $K_2Au_2P_2Se_6$ (IV). $K_2Au_2P_2Se_6$ was synthesized from a less Lewis basic mixture of Au (0.3 mmol), P_2Se_5 (0.3 mmol), K_2Se (0.33 mmol), and Se (3.0 mmol) that was sealed under vacuum in a Pyrex tube and heated to 460 °C for 4 d followed by cooling to 150 °C at 4 °C h^{-1}. The excess $A_x[P_ySe_z]$ flux was removed as above to reveal red rods (72% yield based on Au). The crystals are air- and water-stable. Microprobe analysis gave an average composition of $K_{1.7}Au_{2.0}P_{1.8}Se_{6.2}$.

Preparation of $Rb_2Au_2P_2Se_6$ (V). $Rb_2Au_2P_2Se_6$ was also synthesized from a less Lewis basic mixture of Au (0.3 mmol), P_2Se_5 (0.3 mmol), Rb_2Se (0.33 mmol), and Se (3.0 mmol) that was sealed under vacuum in a Pyrex tube and heated as in **IV**. The excess $A_xP_ySe_z$ flux was removed as above to reveal red rods (55% yield based on Au). The crystals are air- and water-stable. Microprobe analysis gave an average composition of $Rb_{1.8}Au_{2.0}P_{1.7}Se_{6.1}$.

Preparation of K_2AuPS_4 (VI). K_2AuPS_4 was synthesized from a mixture of Au (0.25 mmol), P_2S_5 (0.50 mmol), K_2S (0.50 mmol), and S (1.5 mmol) that was sealed under vacuum in a Pyrex tube. The reaction mixture was heated to 500 °C for 4 days, followed by cooling to 100 °C at a rate of 4 °C/h. The product, which is stable in water and air, was isolated by dissolving the K_2S_x flux with degassed methanol under inert atmosphere to give yellow crystals and chunky yellow crystalline $K_x[P_yS_z]$ flux. The latter was removed by washing with degassed distilled water, followed by methanol and ether to give yellow crystals (75% yield based on Au). Microprobe analysis on single crystals gave an average composition of $K_{1.8}AuP_{1.4}S_{5.6}$.

Preparation of Rb_2AuPS_4 (VII). A mixture of Au (0.25 mmol), P_2S_5 (0.50 mmol), Rb_2S (0.50 mmol), and S (1.5 mmol) was sealed under vacuum in a Pyrex tube and heated as in **VI**. The product, which is stable in air and water, was isolated as in **VI** to give yellow crystals (52% yield based on Au). Microprobe analysis gave an average composition of $Rb_{1.5}AuP_{1.1}S_{5.1}$.

Preparation of Cs_2AuPS_4 (VIII). A mixture of Au (0.25 mmol), P_2S_5 (0.50 mmol), Cs_2S (0.50 mmol), and S (1.5 mmol) was sealed under vacuum in a Pyrex tube and heated as in **VI**. The product, which is stable in water and air, was isolated as in **VI** to give colorless transparent crystals (63% yield based on Au). Microprobe analysis gave an average composition of $Cs_{2.25}AuP_{3.8}S_{6.1}$.

Preparation of $KAuP_2S_7$ (IX). $KAuP_2S_7$ was synthesized from a more acidic Lewis mixture of Au (0.50 mmol), P_2S_5 (0.75 mmol), K_2S (0.50 mmol), and S (1.5 mmol) that was sealed under vacuum in a Pyrex tube. The reaction mixture was heated to 400 °C for 4 days, followed by cooling to 110 °C at a rate of 4 °C/h. The product, which disintegrates in the presence of water, was isolated with degassed methanol to give dark red crystals (50% yield based on Au). The crystals are soluble in DMF forming an orange-red solution. Microprobe analysis gave an average composition of $K_{1.0}Au_{1.2}P_{2.6}S_{10}$.

Preparation of $RbAuP_2S_7$ (X). $RbAuP_2S_7$ was also synthesized from a more acidic Lewis mixture of Au (0.50 mmol), P_2S_5 (0.75 mmol), K_2S (0.50 mmol), and S (1.5 mmol) that was sealed under vacuum in a Pyrex tube and heated as in **IX**. The product, which disintegrates in the presence of water, was isolated as in **IX** to give dark red crystals (50% yield based on Au). These crystals are also soluble in DMF forming an orange-red solution. Microprobe analysis gave an average composition of $Rb_{1.0}Au_{1.2}P_{2.6}S_{9.2}$.

2.3. Physical Measurements. Powder X-ray Diffraction. Analyses were performed using a calibrated Rigaku-Denki/RW400F2 (Rotaflex) rotating anode powder diffractometer controlled by an IBM computer, operating at 45 kV/100 mA and with a 1°/min scan rate, employing Ni-filtered Cu radiation in a Bragg−Brentano geometry. Powder patterns were calculated with the CERIUS^2 software.[13] Calculated and observed XRD patterns are deposited with the Supporting Information.

Infrared Spectroscopy. Infrared spectra, in the far-IR region (600−50 cm^{-1}), were recorded in 4 cm^{-1} resolution on a computer-controlled Nicolet 750 Magna-IR Series II spectrophotometer equipped with a TGS/PE detector and a silicon beam splitter. The samples were ground with dry CsI into a fine powder and pressed into translucent pellets.

Raman Spectroscopy. Raman spectra, in the far-Raman region (700−100 cm^{-1}), were recorded on a BIO-RAD FT Raman spectrometer equipped with a Spectra-Physics Topaz T10-106c 1.064 nm YAG laser and a Ge detector. The samples were ground into a fine powder and loaded into glass tubes.

(13) CERIUS^2, Version 1.6, Molecular Simulations Inc., Cambridge, England, 1994.

Table 1. Crystallographic Data for **I**, **IV**, **VI**, **VIII**, and **IX**

	formula				
	$K_3AuP_2Se_8$ (**I**)	$K_2Au_2P_2Se_6$ (**IV**)	K_2AuPS_4 (**VI**)	Cs_2AuPS_4 (**VIII**)	$KAuP_2S_7$ (**IX**)
fw	1007.89	1007.84	434.25	621.99	522.43
a, Å	7.122(2)	12.289(2)	6.518(2)	6.904(3)	7.917(3)
b, Å	12.527(3)	7.210(1)	6.747(2)	20.093(6)	9.247(2)
c, Å	18.666(4)	8.107(1)	9.468(3)	7.025(5)	14.968(3)
α, deg	90.00	90.00	90.00	90.00	90.00
β, deg	96.06(2)	115.13(1)	92.98(2)	90.00	91.84(9)
γ, deg	90.00	90.00	90.00	90.00	90.00
Z; *V*, Å^3	4; 1655.9(7)	2; 650.3(2)	4; 415.8(2)	8; 974.6(8)	4; 1095.2(8)
λ(Mo Kα), Å	0.710 69	0.710 69	0.710 69	0.710 69	0.710 69
space group	*Cc* (No. 9)	*C*2/*m* (No. 12)	$P2_1/m$ (No. 11)	*Pbcm* (No. 57)	*C*2/*c* (No. 15)
D_{calc}, g/cm^3	4.043	5.147	3.469	4.329	3.168
μ, cm^{-1}	271.86	399.36	196.98	232.71	152.84
$2\theta_{max}$, deg	50	50	50	50	50
temp, °C	23	25	23	−120	23
final R/R_w,[a] %	3.4/3.8	4.5/5.4	2.3/3.0	4.7/3.9	1.6/2.2

[a] $R = \sum(|F_o| - |F_c|)/\sum|F_o|$. $R_w = \{\sum w(|F_o| - |F_c|)^2/\sum w|F_o|^2\}^{1/2}$.

Solid-State UV/Vis/Near-IR Spectroscopy. Optical diffuse reflectance measurements were performed at room temperature using a Shimadzu UV-3101PC double beam, double monochromator spectrophotometer. The instrument is equipped with an integrating sphere and controlled by a personal computer. $BaSO_4$ was used as a 100% reflectance standard for all materials. Samples were prepared by grinding them to a fine powder and spreading them on a compacted surface of the powdered standard material, preloaded into a sample holder.

The reflectance versus wavelength data generated were used to estimate a material's band gap by converting reflectance to absorption data as described earlier.[14]

Single-Crystal Optical Transmission Spectroscopy. Room-temperature single-crystal optical transmission spectra were obtained on a Hitachi U-6000 microscopic FT spectrophotometer mounted on an Olympus BH2-UMA metallurgical microscope over a range 380−900 nm. Crystals lying on a glass slide were positioned over the light source, and the transmitted light was detected from above.

Differential Thermal Analysis (DTA). DTA experiments were performed on a computer-controlled Shimadzu DTA-50 thermal analyzer. Typically a sample (∼25 mg) of ground crystalline material was sealed in quartz ampules under vacuum. A quartz ampule of equal mass filled with Al_2O_3 was sealed and placed on the reference side of the detector. The samples were heated to the desired temperature at 10 °C/min, then isothermed for 10 min, and finally cooled to 50 °C at the same rate. Residues of the DTA experiments were examined by X-ray powder diffraction. To evaluate congruent melting we compared the X-ray powder diffraction patterns before and after the DTA experiments. The stability/reproducibility of the samples were monitored by running multiple heating/cooling cycles.

Semiquantitative Microprobe Analyses. The analyses were performed using a JEOL JSM-6400V scanning electron microscope (SEM) equipped with a TN 5500 EDS detector. Data acquisition was performed with an accelerating voltage of 20 kV and 30 s accumulation time.

Single-Crystal X-ray Crystallography. Intensity data for **I**−**VII** and **IX** were collected using a Rigaku AFC6S four-circle automated diffractometer equipped with a graphite crystal monochromator. Intensity data for **VIII** were collected using a Nicolet (Siemens) four-circle automated diffractometer equipped with a graphite crystal monochromator. Crystal stability was monitored with three standard reflections whose intensities were checked every 150 reflections, and unless noted, no crystal decay was detected in any of the compounds. The space groups were determined from systematic absences and intensity statistics. An empirical absorption correction based on *ψ* scans was applied to all data during initial stages of refinement. An empirical DIFABS correction was applied as recommended[15] after full isotropic refinement, after which full anisotropic refinement was performed. The structures were solved by direct methods using SHELXS-86 software[16a] (for all compounds), and full-matrix least-squares refinement was performed using the TEXSAN software package.[16b] After full refinement the final R/R_w values for $K_3AuP_2Se_8$ were 3.4/3.8%. Since the structure is noncentrosymmetric, refinement was attempted on the other enantiomorph which converged with $R/R_w = 3.9/4.5\%$. Accordingly, the first solution was retained. The $K_2Au_2P_2Se_6$ crystal habit to grow as rods that consist of very thin needles complicated the selection of an appropriate single crystal. The great majority of these crystals gave $a = 6.145(1)$ Å, which is only half the correct length. Long exposure axial photographs revealed weak spots indicating the presence of a $2 \times \alpha$ supercell, but the supercell reflections were too weak to collect. Consequently, many crystals were tested (about 15), until one with strong enough reflections was discovered.

The complete data collection parameters and details of the structure solution and refinement for **I**, **IV**, **VII**, **VIII**, and **IX** are given in Table 1. The coordinates of all atoms, average temperature factors, and their estimated standard deviations are given in Tables 2−6.

Table 2. Positional Parameters and B_{eq}[a] Values for $K_3AuP_2Se_8$

atom	*x*	*y*	*z*	B_{eq},[a] Å^2
Au	1	0.0491(1)	$^1/_2$	2.18(5)
Se(1)	1.0751(5)	0.0041(3)	0.6258(2)	2.4(2)
Se(2)	1.4795(6)	−0.1416(3)	0.7198(2)	3.0(2)
Se(3)	1.5538(5)	0.0433(3)	0.5764(2)	2.7(2)
Se(4)	1.3189(5)	−0.2216(3)	0.5597(2)	2.2(2)
Se(5)	1.2172(5)	−0.1695(3)	0.4415(2)	2.5(2)
Se(6)	1.2294(5)	0.3177(3)	0.4193(2)	2.5(2)
Se(7)	0.9173(5)	0.0907(3)	0.3742(2)	2.6(2)
Se(8)	1.3382(5)	0.1570(3)	0.7767(2)	2.6(2)
K(1)	1.794(1)	0.1037(7)	0.7457(5)	3.7(4)
K(2)	1.307(1)	0.2752(7)	0.6039(5)	3.4(4)
K(3)	1.432(1)	0.0695(7)	0.3939(5)	3.2(4)
P(1)	1.365(1)	−0.0638(7)	0.6227(5)	1.9(3)
P(2)	0.951(1)	0.2681(7)	0.3767(4)	1.6(3)

[a] *B* values for anisotropically refined atoms are given in the form of the isotropic equivalent displacement parameter defined as $B_{eq} = (4/3)[a^2B(1,1) + b^2B(2,2) + c^2B(3,3) + ab(\cos\gamma)B(1,2) + ac(\cos\beta)B(1,3) + bc(\cos\alpha)B(2,3)]$.

3. Results and Discussion

3.1. Description of Structures. $A_3AuP_2Se_8$ (I−III) are isostructural, but since the single-crystal structure determination was performed on the K^+ salt (**I**), the discussion will refer mainly to this compound. The novel one-dimensional structure

(14) McCarthy, T. J.; Ngeyi, S.-P.; Liao J.-H.; DeGroot, D.; Hogan, T.; Kannewurf, C. R.; Kanatzidis, M. G. *Chem. Mater.* **1993**, *5*, 331−340.

(15) Walker, N.; Stuart, D. *Acta Crystallogr.* **1983**, *A39*, 158.

(16) (a) Sheldrick, G. M. In *Crystallographic Computing 3*; Sheldrick, G. M., Kruger, C., Doddard, R., Eds.; Oxford University Press: Oxford, England, 1985; p 175. (b) Gilmore G. J. *Appl. Crystallogr.* **1984**, *17*, 42−46.

Table 3. Positional Parameters and B_{eq} Values for $K_2Au_2P_2Se_6$

atom	*x*	*y*	*z*	B_{eq}, Å^2
Au	0	0.2564(2)	0	1.15(4)
Se(1)	−0.2144(3)	0	0.1994(4)	1.7(1)
Se(2)	0.0727(2)	0.2531(3)	0.3262(3)	1.89(8)
P	−0.0224(6)	0	0.350(1)	0.7(2)
K	0.2988(7)	0	0.260(1)	2.5(3)

Table 4. Positional Parameters and B_{eq} Values for K_2AuPS_4 with Estimated Standard Deviations in Parentheses

atom	*x*	*y*	*z*	B_{eq}, Å^2
Au	1	0	0	1.46(2)
K(1)	1.4551(5)	1/4	−0.1657(3)	2.7(1)
K(2)	0.7958(4)	1/4	0.4641(3)	1.8(1)
S(1)	1.5245(5)	1/4	0.1742(3)	2.0(1)
S(2)	1.3050(5)	1/4	0.4926(3)	1.6(1)
S(3)	1.0927(3)	−0.0034(3)	0.2370(2)	1.78(8)
P	1.2650(4)	1/4	0.2804(3)	1.0(1)

Table 5. Positional Parameters and B_{eq} Values for Cs_2AuPS_4 with Estimated Standard Deviations in Parentheses

atom	*x*	*y*	*z*	B_{eq}, Å^2
Au	0.1130(2)	1/4	0	1.19(5)
Cs(1)	0.7921(3)	0.4850(1)	1/4	1.26(8)
Cs(2)	0.3957(3)	0.6646(1)	1/4	2.0(1)
S(1)	0.529(1)	0.3390(4)	1/4	1.4(3)
S(2)	0.1137(7)	0.3637(2)	0.0047(9)	1.2(2)
S(3)	0.297(1)	0.4860(4)	1/4	1.2(3)
P	0.276(1)	0.3871(4)	1/4	1.0(3)

Table 6. Positional Parameters and B_{eq} Values for $K_2AuP_2S_7$ with Estimated Standard Deviations in Parentheses

atom	*x*	*y*	*z*	B_{eq}, Å^2
Au	1/4	1/4	0	1.48(1)
K	1/2	0.2534(3)	1/4	5.1(1)
S(1)	0.2212(2)	0.4202(2)	0.1153(1)	2.01(6)
S(2)	−0.0310(2)	0.1920(2)	0.0324(1)	2.06(6)
S(3)	0	0.1872(2)	1/4	1.83(8)
S(4)	−0.1959(2)	0.4716(2)	0.1542(1)	2.39(6)
P	−0.0133(2)	0.3328(2)	0.1388(1)	1.56(5)

is shown in Figure 1. The monovalent Au cation is linearly coordinated. This class of compounds expands the repertoire of the (poly)selenophosphate ligands introducing the new $[P_2Se_8]^{4-}$ unit. To the best of our knowledge, this is the first example of the $[P_2Se_8]^{4-}$ unit in a selenophosphate compound. The $[P_2Se_8]^{4-}$ unit is formed by the condensation of two $[PSe_4]^{3-}$ units through the formation of a Se−Se bond. Kolis et al.[17] have observed the related $[P_2Se_8]^{2-}$, which consists of a six-membered P_2Se_4 ring with each phosphorus atom containing two terminal selenide atoms; see Chart 1.

The sulfur analog $[P_2S_8]^{4-}$ has been observed in the ternary thiophosphates PV_2S_{10}[18] and PNb_2S_{10}.[19] In those compounds the $[P_2S_8]^{4-}$ unit is coordinatively saturated, whereas in **I**−**III** only two coordination sites of the $[P_2Se_8]^{4-}$ are utilized [Se(1), Se(7)] presumably because of the low coordination preference of the gold centers. In this way, every $[P_2Se_8]^{4-}$ group links two Au centers creating infinite zigzag $[AuP_2Se_8]_n^{3n-}$ chains. These chains run in [110] and [2$\bar{2}$0] directions and are almost mutually perpendicular to each other, in a crisscross fashion, an unusual packing for 1-D compounds. Another interesting feature of this arrangement is that it crystallizes in a polar noncentrosymmetric space group, which makes the compound

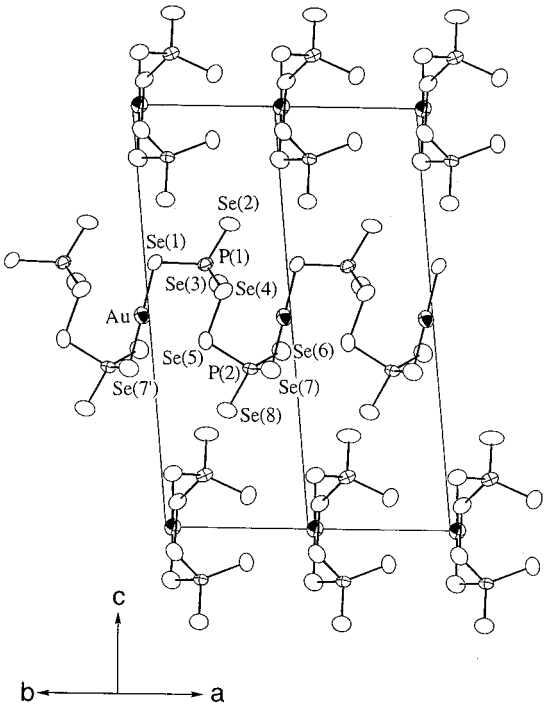

Figure 1. ORTEP representation and labeling of $K_3AuP_2Se_8$ in a diagonal view. Cations have been omitted for clarity (80% probability ellopsoids).

Chart 1

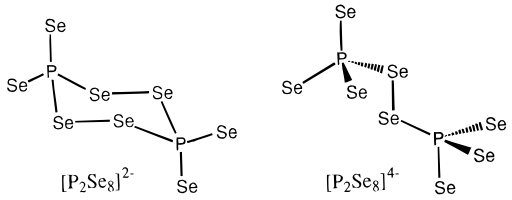

a possible candidate for nonlinear optical measurements. The polarity of the structure can be easily seen by inspecting the perpendicular chains in Figure 1, which in a projection resemble the letter "C". In the same figure one can observe that all the "C"s face the same direction. The Au−Se distances have an average value of 2.418(4) Å and compare very well with those found in $Rb_2AuP_2Se_6$,[12] $KAuSe_5$,[20a] and $CsAuSe_3$,[20b] all featuring linearly coordinated Au^+. The P−Se distances range from 2.141(9) to 2.307(9) Å with the terminal selenium atoms displaying the shorter distances. The torsion angle around Se(4)−Se(5) is 117.1(3)°. The $[AuP_2Se_8]_n^{3n-}$ chains are separated by A^+ ions that are located in three different sites. In $K_3AuP_2Se_8$, K(1) is coordinated by six Se atoms [range of K(1)−Se distances, 3.394(9)−3.51(1) Å; average 3.462 Å], K(2) is also six-coordinate [3.45(1)−3.54(1) Å; average 3.484 Å], and K(3) is seven-coordinate [3.424(9)−3.654(9) Å; average 3.520 Å]. Tables of selected distances and angles for $K_3AuP_2Se_8$ are given in Table 7.

$K_2Au_2P_2Se_6$ (IV) and $Rb_2Au_2P_2Se_6$ (V). These two compounds are isostructural, but since the single-crystal structure determination was performed on the K^+ salt (**IV**), the discussion will refer mainly to this compound. The one-dimensional structure is shown in Figure 2. The chains propagate along the [001] direction. The monovalent Au is also linearly coordinated. The structure features the ethane-like $[P_2Se_6]^{4-}$ unit. The

(17) Zhao, J.; Pennington, W. T.; Kolis, J. W. *J. Chem. Soc., Chem. Commun*. **1992**, 265−266.
(18) Brec, R.; Ouvrard, G.; Evain, M.; Grenouilleau, P.; Rouxel, J. *J. Solid State Chem.* **1983**, *47*, 174−184.
(19) Brec, R.; Grenouilleau, P.; Evain, M.; Rouxel, J. *Rev. Chim. Miner*. **1983**, *20*, 295−304.
(20) (a) Park, Y.; Kanatzidis, M. G. *Angew. Chem., Int. Ed. Engl.* **1990**, *29*, 914−915. (b) Park, Y. Ph.D. Dissertation, Michigan State University, E. Lansing, MI, 1991.

Table 7. Selected Distances (Å) and Angles (deg) for $K_3AuP_2Se_8$ with Standard Deviations in Parentheses[a]

Se(1)−P(1)	2.242(9)	Au−Se(1)	2.419(4)
Se(2)−P(1)	2.141(9)	Au−Se(7′)	2.417(4)
Se(3)−P(1)	2.143(9)		
Se(4)−P(1)	2.307(9)	Se(4)−Se(5)	2.342(6)
Se(5)−P(2)	2.295(9)		
Se(6)−P(2)	2.150(8)		
Se(7)−P(2)	2.235(9)		
Se(8)−P(2)	2.165(9)		
Se(1)−Au−Se(7)	178.4(1)	Au−Se(1)−P(1)	100.0(3)
Se(4)−Se(5)−P(2)	103.5(3)		
Se(5)−Se(4)−P(1)	104.8(3)		
Se(1)−P(1)−Se(2)	114.8(4)	Se(5)−P(2)−Se(6)	113.5(4)
Se(1)−P(1)−Se(3)	113.0(4)	Se(5)−P(2)−Se(7)	105.5(4)
Se(1)−P(1)−Se(4)	104.8(3)	Se(5)−P(2)−Se(8)	94.8(3)
Se(2)−P(1)−Se(3)	115.4(4)	Se(6)−P(2)−Se(7	112.8(4)
Se(2)−P(1)−Se(4)	93.6(3)	Se(6)−P(2)−Se(8)	115.9(4)
Se(3)−P(1)−Se(4)	113.2(4)	Se(7)−P(2)−Se(8)	112.6(4)

[a] The estimated standard deviations in the mean bond lengths and the mean bond angles are calculated by the equation $\sigma(l) = \{\sum_n (l_n - l)^2/n(n-l)\}^{1/2}$, where l_n is the length (or angle) of the nth bond, l the mean length (or angle), and n the number of bonds.

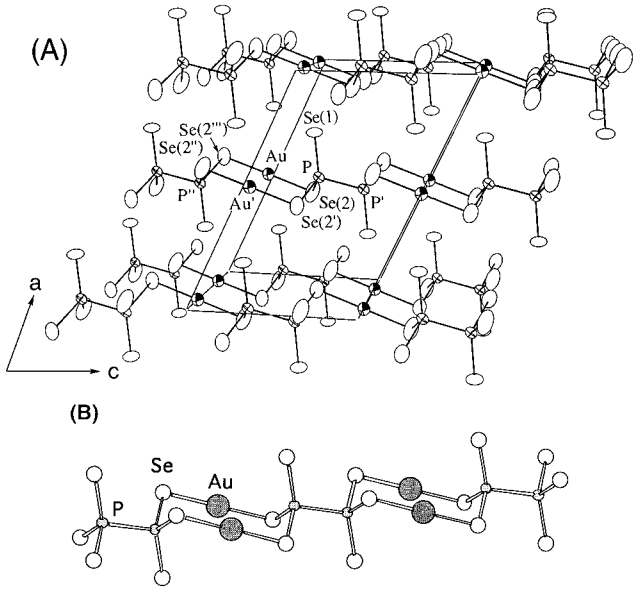

Figure 2. (A) ORTEP representation and labeling of $K_2Au_2P_2Se_6$ looking down the *b*-axis. Cations have been omitted for clarity (90% probability ellopsoids). (B) View of a single $[Au_2P_2Se_6]^{2n-}$ chain.

Chart 2

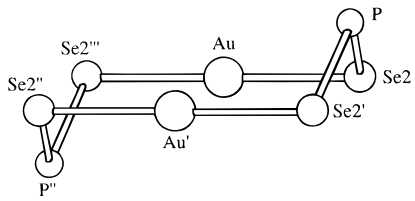

formation of the P−P bond reduces the oxidation state of the phosphorus from P^{5+} (as observed in $[P_2Se_8]^{4-}$) to P^{4+}. The presence of this unit was expected since low flux basicity was used for the synthesis of $A_2Au_2P_2Se_6$ (see 3.2. Synthesis). The $[P_2Se_6]^{4-}$ adopts the staggered conformation and employs four selenium atoms (two from each phosphorus) to coordinate with four Au^+ centers forming an interesting pseudocyclohexane ring in a chair configuration as shown in Chart 2. A similar, though rather distorted, ring conformation has been observed for the molecular $[Au_2(WS_4)_2]^{2-}$.[21]

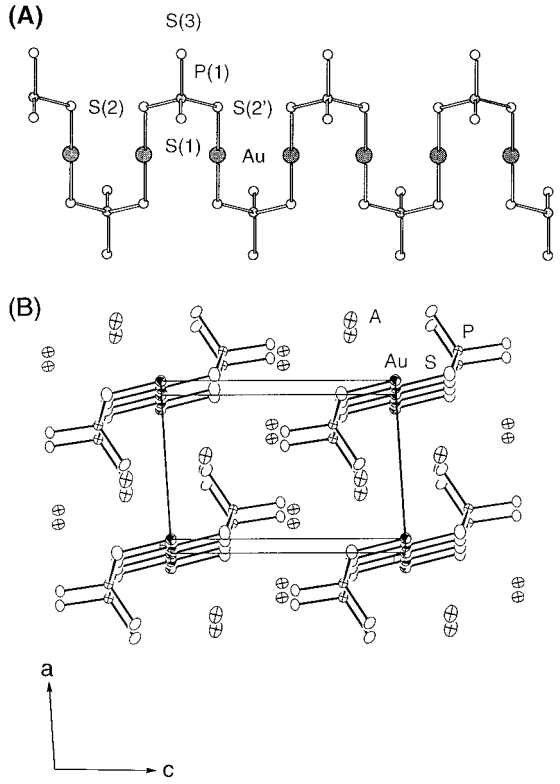

Figure 3. (A) View of a single $[AuPS_4]^{2n-}$ chain with labeling. (B) ORTEP representation of K_2AuPS_4 as viewed down the *b*-axis (50% probability ellopsoids).

Table 8. Selected Distances (Å) and Angles (deg) for $K_2Au_2P_2Se_6$ with Standard Deviations in Parentheses

Se(1)−P	2.147(8)	Au−Se(2)	2.405(2)
Se(2)−P	2.221(4)		
P−P′	2.25(1)	Au−Au′	3.697(3)
Se(2)−Au−Se(2‴)	178.9(1)	Au−Se(2)−P	98.2(2)
Se(1)−P−Se(2)	116.2(2)	Se(1)−P−P′	108.8(4)
Se(2)−P−Se(2′)	110.5(3)	Se(2)−P−P′	101.5(3)

Table 9. Selected Distances (Å) and Angles (deg) for K_2AuPS_4 with Standard Deviations in Parentheses

P(1)−S(1)	2.012(4)	S(1)−P(1)−S(2)	115.5(2)
P(1)−S(2)	2.013(4)	S(1)−P(1)−S(3)	111.2(1)
P(1)−S(3)	2.075(3) (×2)	S(1)−P(1)−S(3′)	111.2(1)
		S(2)−P(1)−S(3)	103.8(1)
Au(1)−S(3)	2.293(2)	S(2)−P(1)−S(3′)	103.8(1)
Au(1)−S(3′)	2.293(2)	S(3)−P(1)−S(3′)	110.9(2)
		S−P−S (mean)	109(1)
Au(1)−Au(1′)	3.373(1)		
S(3)−Au(1)−S(3)	180.00	Au(1)−S(3)−P(1)	107.3(1)

There is a crystallographic center of symmetry located in the middle of every P−P bond (P−P distance is 2.25(1) Å). The staggered conformation and the way the ligand coordinates dictate the "staircase" chain propagation (see Figure 2). The Au−Au′ distance in this ring is 3.697(3) Å, which does not indicate any significant interactions. The Au−Se(2) distance is 2.405(2) Å and compares very well with those mentioned above. The P−Se(1) distance is 2.147(4) Å, shorter than the P−Se(2) distance of 2.221(4) Å. The $[Au_2P_2Se_6]_n^{2n-}$ chains are separated by six-coordinated A^+ ions [for $K_2Au_2P_2Se_6$, range of K−Se distances, 3.413(9)−3.640(7) Å; average 3.566 Å]. Selected distances and angles for $K_2Au_2P_2Se_6$ are given in Table 8.

(21) Muller, A.; Dornfeld, H.; Henkel, G.; Krebs, B.; Viegers, M. P. A. *Angew. Chem., Int. Ed. Engl.* **1978**, *17*, 52.

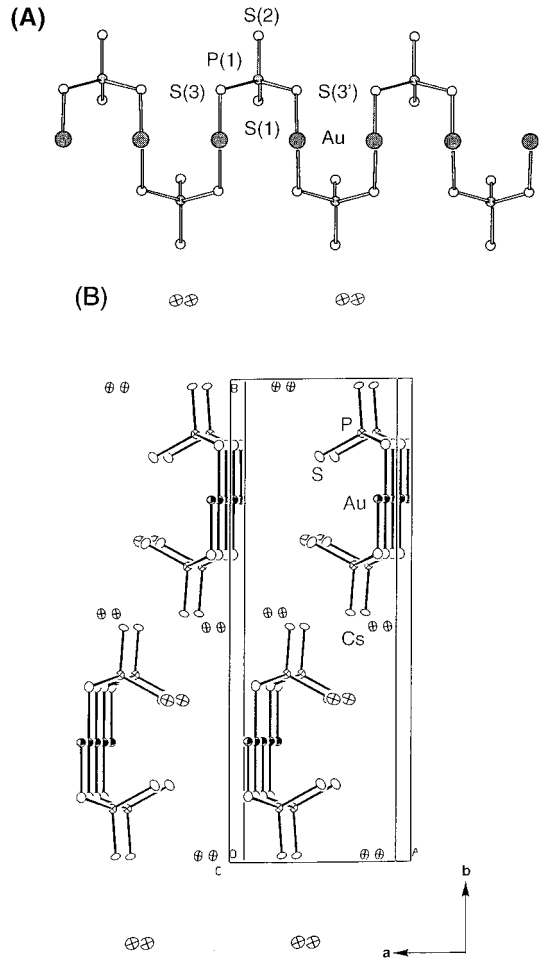

Figure 4. (A) View of a single $[AuPS_4]^{2n-}$ chain with labeling. (B) ORTEP representation of Cs_2AuPS_4 as viewed down the *c*-axis (50% probability ellopsoids).

Table 10. Selected Distances (Å) and Angles (deg) for Cs_2AuPS_4 with Standard Deviations in Parentheses

P(1)−S(1)	2.00(1)	Au(1)−S(2)−P(1)	103.6(3)
P(1)−S(2)	2.108(7) (×2)		
P(1)−S(3)	1.99(1)	S(2)−Au(1)−S(2)	179.8(3)
P(1)−S(mean)	2.05(3)		
		S(1)−P(1)−S(2)	110.9(3) (×2)
Au(1)−S(2)	2.285(5) (×2)	S(1)−P(1)−S(3)	114.8(5)
		S(2)−P(1)−S(2′)	109.7(4)
Au(1)−Au(1′)	3.427(1)	S(2)−P(1)−S(3)	105.1(3) (×2)

K_2AuPS_4 (VI) and Rb_2AuPS_4 (VII). These two compounds are isostructural. The single-crystal structure determination was performed on the K^+ salt (**VI**), and so the discussion will refer mainly to this compound. The structure of the $[AuPS_4]_n^{2n-}$ anion is one-dimensional built of alternating $[PS_4]^{3-}$ tetrahedra linked in a corner-sharing fashion to monovalent Au atoms. The chains run along the crystallographic *b*-axis (Figure 3A) and are separated by alkali metal cations (Figure 3B). The chains are propagated by a crystallographic screw axis resulting in the terminal sulfides of the $[PS_4]^{3-}$ ligand to appear on opposite sides of the S−Au−S linkage. It is interesting to note that this structural motif is not observed in **I**−**III**. The S−Au−S angle is constrained by symmetry to be linear. The Au resides on an inversion center with an average Au−S distance of 2.293(2) Å. This compares well with the Au−S distance found in $KAuS_5$,[20a] $K_2Au_2SnS_4$,[20b] $K_2Au_2Sn_2S_6$,[22] $BaAu_2SnS_4$,[23] and $K_4Au_6S_5$,[24] all featuring linearly coordinated Au^+. The $[PS_4]^{3-}$ ligand is a regular tetrahedron with an average P−S bond distance of 2.04(1) Å and mean S−P−S angle of 109(2)°, respectively. The $[PS_4]^{3-}$ tetrahedra are in a staggered arrangement above and below the Au−S linear bond (see Figure 3B). The Au−Au′ distance is 3.598(2) Å suggesting no significant bonding interactions. Selected bond distances and angles for K_2AuPS_4 are given in Table 9. The A^+ ions are located in two different sites. In K_2AuPS_4, K(1) is coordinated by six S atoms [range of K(1)−S distances, 3.227(4)−3.481(4) Å; average 3.37(3) Å] and K(2) is eight-coordinate [3.186(4)−3.424(3) Å; average 3.35(4) Å].

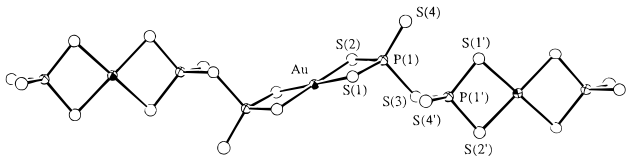

Figure 5. ORTEP representation and labeling of a single $[AuP_2S_7]^{n-}$ chain (50% probability ellopsoids).

Table 11. Selected Distances (Å) and Angles (deg) for $K_2AuP_2S_7$ with Standard Deviations in Parentheses

P(1)−S(1)	2.065(2)	S(1)−Au(1)−S(1′)	180.00
P(1)−S(2)	2.058(2)	S(1)−Au(1)−S(2)	83.49(5) (×2)
P(1)−S(3)	2.140(2)	S(1′)−Au(1)−S(2′)	96.51(5) (×2)
P(1)−S(4)	1.952(2)	S(2)−Au(1)−S(2′)	180.00
P(1′)−S(3)	2.140(2)		
		Au(1)−S(1)−P(1)	88.40(7) (×2)
Au(1)−Au(1′)	6.086(1)	Au(1)−S(2)−P(1)	88.52(7) (×2)
Au(1)−S(1)	2.352(2) (×2)	S(1)−P(1)−S(2)	98.90(8)
Au(1)−S(2)	2.354(2) (×2)	S(1)−P(1)−S(3)	110.90(8)
		S(1)−P(1)−S(4)	115.8(1)
P(1)−S(3)−P(1′)	102.1(1)	S(2)−P(1)−S(3)	101.79(9)
		S(2)−P(1)−S(4)	118.3(1)
		S(3)−P(1)−S(4)	109.87(8)
		S−P−S (mean)	109(3)

Cs_2AuPS_4 (VIII). The structure of the $[AuPS_4]_n^{2n-}$ anion is closely related to that of **I**−**III** (see Figure 1). The chains run along the crystallographic *c*-axis (Figure 4A) and are separated by alkali cations (Figure 4B). The overall $[AuPS_4]_n^{2n-}$ chain structure is related to $A_3AuP_2Se_8$, and its projection also resembles the letter "C". The difference is the reduction of the diselenide bridge of the $[P_2Se_8]^{4-}$ group by a second S−Au−S linkage, creating two $[PS_4]^{3-}$ units. Although the chain structure is similar to that of **I**−**III**, the chains stack in a centrosymmetric parallel fashion instead of the unusual crisscross packing motif observed in **I**−**III**. The ribbons are isostructural to A_2AuSbS_4 (A = Rb, Cs)[25] and are propagated by a crystallographic glide plane resulting in the terminal sulfides of the $[PS_4]^{3-}$ ligand to appear on the same side of the essentially linear S−Au−S linkage forming a projection resembling the letter "C". The S−Au−S angle is essentially linear, at 178.9(2)°. The Au atom resides on a 2-fold crystallographic site with a Au−S distance of 2.285(2) Å. The $[PS_4]^{3-}$ unit binds to two monovalent Au cations leaving the other sulfides terminal. The $[PS_4]^{3-}$ unit is a regular tetrahedron with an average P−S bond distance of 2.05(3) Å and mean S−P−S angles of 109(2)°. The $[PS_4]^{3-}$ tetrahedra are in a staggered arrangement above and below the S−Au−S linear bond. The Au−Au′ distance is 3.667(2) Å indicating no significant bonding interaction. Selected bond distances and angles for Cs_2AuPS_4 are given in Table 10. The $[AuPS_4]_n^{2n-}$ chains are separated by Cs^+ ions that are located in two different sites. In Cs_2AuPS_4, Cs(1) is coordinated by

(22) Liao, J.-H.; Kanatzidis, M. G. *Chem. Mater.* **1993**, *5*, 1561.
(23) Teske, Chr. L. *Z. Anorg. Allg. Chem.* **1978**, *445*, 193−201.
(24) Klepp, K. O.; Bronger, W. *J. Less Common Met.* **1988**, *137*, 13−20.
(25) Hanko, J. A.; Kanatzidis, M. G. Manuscript in preparation.

Table 12. Synthetic Conditions for the Different $[P_yQ_z]^{n-}$ Units (M = Metal, A_2Q = Alkali Metal Chalcogenide)

reactant ratio $M/P_2Se_5/A_2Se/Se$	P^{n+}/ligands	temp, °C	refs
1/1−3/1−2/10	$P^{4+}/[P_2Se_6]^{4-}$	410−510	1, 4, 5, 9, 12, present work
1/1.5−2/3−4/10	$P^{5+}/[PSe_4]^{3-}$, $[PSe_5]^{3-}$, $[P_2Se_8]^{4-}$	440−450	6, 8, present work
1/2−3/2/10	$P^{5+}/[P_2Se_7]^{4-}$, $[P_2Se_9]^{4-}$	490	7
$M/P_2S_5/A_2S/S$			
1/1.5−3/2−4/4−12	$P^{5+}/[PS_4]^{3-}$, $[P_2S_7]^{4-}$	400−500	2, 3, present work
1/3/2/4	$P^{4+}/[P_2S_6]^{4-}$	400	3

Table 13. Optical Band Gap, Color, and Melting Point Data

formula	E_g, eV	color	mp, °C
$K_3AuP_2Se_8$	2.14	yellow-orange	442
$Rb_3AuP_2Se_8$	2.22	yellow	483
$Cs_3AuP_2Se_8$	2.24	yellow	478
$K_2Au_2P_2Se_6$	1.93	red	517[a]
$Rb_2Au_2P_2Se_6$	1.95	red	519[a]
K_2AuPS_4	2.50	yellow	498
Rb_2AuPS_4	2.59	yellow	418
Cs_2AuPS_4	3.04	colorless	375[a,b]
$KAuP_2S_7$	2.09	dark red	398
$RbAuP_2S_7$	2.15	dark red	404[a]

[a] Incongruent melting [b] Converts to β-Cs_2AuPS_4, isotypic to K_2AuPS_4.

nine S atoms [range of Cs(1)−S distances, 3.394(9)−3.51(1) Å; average 3.57(3) Å] and Cs(2) is eight-coordinate [3.45(1)−3.54(1) Å; average 3.75(7) Å].

$KAuP_2S_7$ (IX) and $RbAuP_2S_7$ (X). These two compounds are isostructural. The single-crystal structure determination was performed on the K^+ salt (**IX**), and so the discussion will refer mainly to this compound. The structure of $[AuP_2S_7]_n^{n-}$ is a unique one-dimensional chain consisting of alternating $[P_2S_7]^{4-}$ units edge-sharing to square planar Au^{3+} cations. Having a d^8 electron configuration, the Au^{3+} atom adopts a square planar coordination environment. The chains run along the $[10\bar{1}]$ direction (Figure 5) and are separated by alkali cations. The Au center resides on an inversion center with Au−S bond distances ranging from 2.352(2) to 2.354(2) Å and P−S distances ranging from 1.952(2) to 2.140(2) Å. The Au−Au′ distance between chains is 6.068(1) Å. Inspection of the S(1)−Au(1)−S(2) angles of 83.49(5) and 96.51(5)° reveals a slight deviation from an ideal square planar geometry, which is due to a strained four-membered (Au(1)−S(1)−P(1)−S(2)) ring. The pyrothiophosphate $[P_2S_7]^{4-}$ unit consists of two corner-sharing $[PS_4]^{3-}$ tetrahedra. The $[P_2S_7]^{4-}$ unit has been observed in the ternary compounds $As_2P_2S_7$,[26] $Hg_2P_2S_7$,[27] $Ag_4P_2S_7$,[28] and $Ag_7(PS_4)(P_2S_7)$.[29] Each PS_4 tetrahedron is slightly distorted with S−P−S angles ranging from 98.90(8) to 118.3(1)°, respectively. The smallest angle is associated with the constrained S−P−S−Au four-membered rings, and the largest, with the terminal sulfide. The chains are separated by alkali metal cations residing in a pocket between the terminal sulfide (S(4)) and a bridging sulfide (S(2)) In $KAuP_2S_7$ the potassium cation is coordinated by six sulfur atoms [range of K(1)−S distances 3.324(2)−3.485(2) Å; average 3.37(3) Å]. Selected bond distances and angles for $KAuP_2S_7$ are given in Table 11.

(26) Hönle, W.; Wibbelmann, C.; Brockner, W. *Z. Natuforsch.* **1984**, *39b*, 1088−1091.
(27) Jandali, V. M. Z.; Eulenberger, G.; Hann, H. *Z. Anorg. Allg. Chem.* **1978**, *445*, 184−192.
(28) Toffoli, P.; Khodadad, P.; Rodier, N. *Acta Crystallogr.* **1977**, *B33*, 1492−1494.
(29) Toffoli, P.; Khodadad, P.; Rodier, N. *Acta Crystallogr.* **1982**, *B38*, 2374−2378.

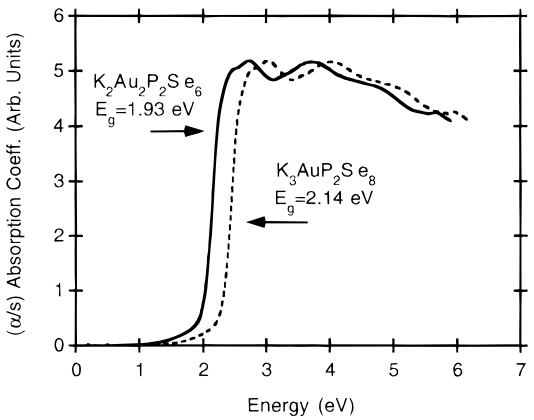

Figure 6. Solid-state optical absorption spectra of $K_3AuP_2Se_8$ (**I**) and $K_2Au_2P_2Se_6$ (**IV**).

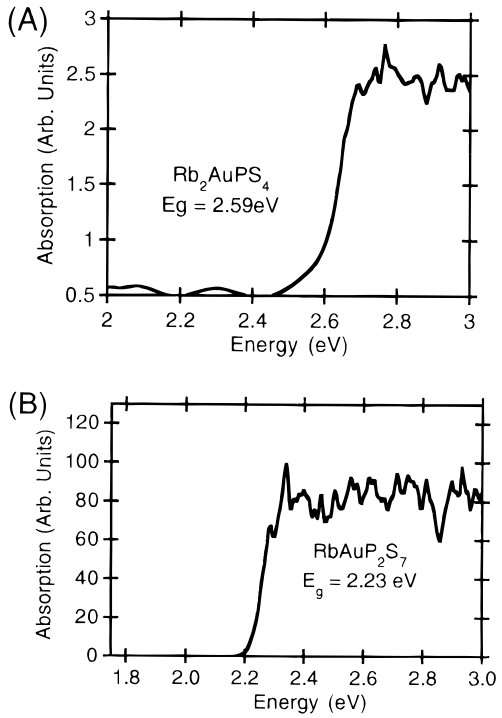

Figure 7. Single-crystal absorption spectra of Rb_2AuPS_4 (**VII**) and $RbAuP_2S_7$ (**X**). The sharp features at high absorbance values are noise due to the very low transmission of light at those energies.

3.2. Synthesis, Spectroscopy, and Thermal Analysis. The syntheses were the result of redox reactions in which the metal is oxidized by polychalcogenide ions in the $A_x[P_yQ_z]$ flux. The Au^{n+} centers are then coordinated by the highly charged $[P_yQ_z]^{n-}$ ligands. The molten polychalcophosphate flux method is very effective for crystal growth in this system. The isolation of pure crystalline products is facilitated by the flux solubility in aqueous and organic solvents. Good control of the Lewis basicity of the flux can be achieved by means of varying the starting composition. Species of either P^{5+} or P^{4+} can be stabilized which results in compounds with different $[P_yQ_z]^{n-}$ ligands.

Our studies with quaternary chalcophosphates provide enough examples for the construction of Table 12 in which we summarize under what conditions each species is stabilized. It is evident that there are differences between thio- and selenophosphates, and we will discuss each case separately. According to the table the most decisive factor controlling the production of P^{5+} or P^{4+} species in the Se flux is the A_2Se content. Using high A_2Se content (basic conditions), exclusively species with

Table 14. Infrared and Raman Data (cm^{-1}) for **I**, **IV**, **VI**, **VIII**, and **IX**

$K_3AuP_2Se_8$ (**I**)		$K_2Au_2P_2Se_6$ (**IV**)		K_2AuPS_4 (**VI**)		Cs_2AuPS_4 (**VIII**)		$KAuP_2S_7$ (**IX**)	
IR	Raman	IR	Raman	IR	Raman	IR	Raman	IR	Raman
499	499		499			619			669
489		477			603			576	
445	446		459	552	551			543	
435	433	434	437					536	
	391	424		519		519			
374	374	288			470		471		
	260	237						458	
	225	227	225		419		410		418
			192	400	395	384	398	387	
	160		147	368		370	363		367
				350	355				
				327				327	325
				303				304	
				289				288	286
				278			271	280	
				268					
				253	257			255	256
				246	241	241	244	240	
				217	217		217	228	
				208				209	210
				202				203	
				196	181		183		
				169		161		170	
					152		150		

P^{5+} are formed. Lowering the A_2Se content (lowering the basicity), favors the stabilization of P^{4+} species and, in particular, the $[P_2Se_6]^{4-}$ ligand. The only exception is Ti which provides species with P^{5+} even under low basicity conditions,[7] which might be an effect of the highly acidic Ti^{4+} cation. The exact influence of each transition metal in the flux on the oxidation state of phosphorus is not understood yet. Attempts to synthesize the hypothetical $AAu^{III}P_2Se_6$ were not successful, and instead the mixed-valent $A_2AuP_2Se_6$[12] or the Au^+ compounds $A_2Au_2P_2Se_6$ were obtained. In the present work basic conditions stabilize the $[P_2Se_8]^{4-}$ ligand and less basic conditions the $[P_2Se_6]^{4-}$.

For the thiophosphates, a wide range of conditions result in the formation of exclusively P^{5+} species. Low P_2S_5 concentrations favored the $[PS_4]^{3-}$ unit, while high concentration of P_2S_5 favored the $[P_2S_7]^{4-}$ unit. A review of the literature revealed only a few structurally characterized quaternary alkali compounds featuring the $[P_2S_6]^{4-}$ unit. Of these compounds, KMP_2S_6 (M = Mn, Fe)[30] was synthesized by direct combination and $Na_{0.16}Bi_{1.28}P_2S_6$,[3] which was produced in a molten thiophosphate flux. In the latter case the use of the less basic Na^+ counterion may be important for the stabilization of P^{4+}.

Structurally, the seleno- and thiophosphates possess differences due mainly to the presence of different ligands. Nevertheless, the $[AuPS_4]_n^{2n-}$ anion in **VIII** is similar to the $[AuP_2Se_8]_n^{3n-}$ anion in **I**−**III**, in that two oxidatively coupled $[PQ_4]^{3-}$ units give a $[P_2Q_8]^{4-}$ group. Even in this case, though there are other essential chemical differences such as the metal/phosphorus ratio (1:1 in **VIII** and 1:2 in **I**−**III**). When the same ligands and the same countercation are present, it is possible to synthesize isostructural compounds. The case of $KTiPSe_5$[7] and $KTiPS_5$[31] represents a rare example where isostructural analogs of both S and Se analogs are known.

The optical absorption properties of **I**−**X** were evaluated by examining the solid-state UV/vis diffuse reflectance and/or single-crystal optical transmission spectra of the materials (see Table 13). The spectra confirm the semiconducting nature of the materials by revealing the presence of sharp optical gaps. The $A_3AuP_2Se_8$ (A = K, Rb, Cs) compounds exhibit steep absorption edges from which the band gap, E_g, can be assessed at 2.14 eV (**I**), 2.22 eV (**II**), and 2.24 eV (**III**), respectively. The band gaps of $A_2Au_2P_2Se_6$ (A = K, Rb) are 1.93 eV (**IV**) and 1.95 eV (**V**), respectively. The energy gap increases slightly with the larger alkali cation size, as expected. Representative spectra for **I** and **IV** are given in Figure 6. The transparent crystals of **VI**−**X** were suitable for single-crystal optical transmission measurements. The band gaps of A_2AuPS_4 (A = K, Rb, and Cs) are 2.51 eV (**VI**), 2.59 eV (**VII**), and 3.04 eV (**VIII**), respectively. The band gaps of $AAuP_2S_7$ occur at 2.03 eV (**IX**) and 2.23 eV (**X**), respectively (see Figure 7). In both cases, the energy gap increases slightly with the larger alkali cation size.

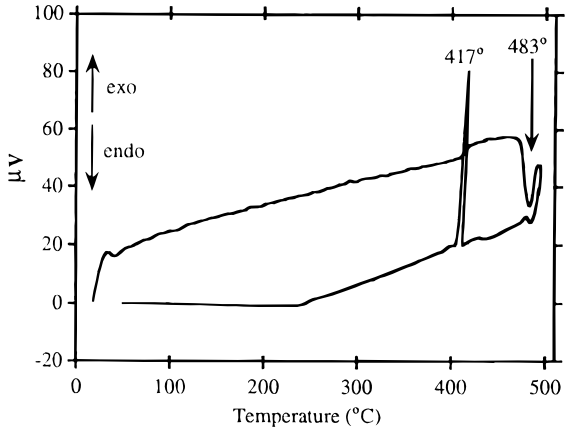

Figure 8. Typical DTA diagram for the $A_3AuP_2Se_8$ phases (A = Rb).

The far-IR and Raman data were in good agreement, and the results are summarized in Table 14. The far-IR spectra of **I**−**III** display absorptions at ∼437 and ∼447 cm^{-1}, which can be assigned to PSe_4 stretching modes,[1,6] but also three more absorptions at ∼501, ∼490, and 376 cm^{-1}, which should be of diagnostic value in distinguishing the $[P_2Se_8]^{4-}$ ligand from the $[PSe_4]^{3-}$. The infrared spectra of **IV** and **V** display absorptions at ∼477, ∼434, ∼421, ∼288, ∼237, and ∼227 cm^{-1} charac-

(30) (a) Menzel, F.; Brockner, W; Carrillo-Cabrera, W.; von Schnering, H. G. *Z. Anorg. Allg. Chem.* **1994**, *620*, 1081−1086. (b) Carrillo-Cabrera, W.; Sabmannshausen, J.; von Schnering, H. G.; Menzel, F.; Brockner, W. *Z. Anorg. Allg Chem.* **1994**, *620*, 489−494.
(31) Do, J.; Lee, K.; Yun, H. *J. Solid State Chem.* **1996**, *125*, 30−36.

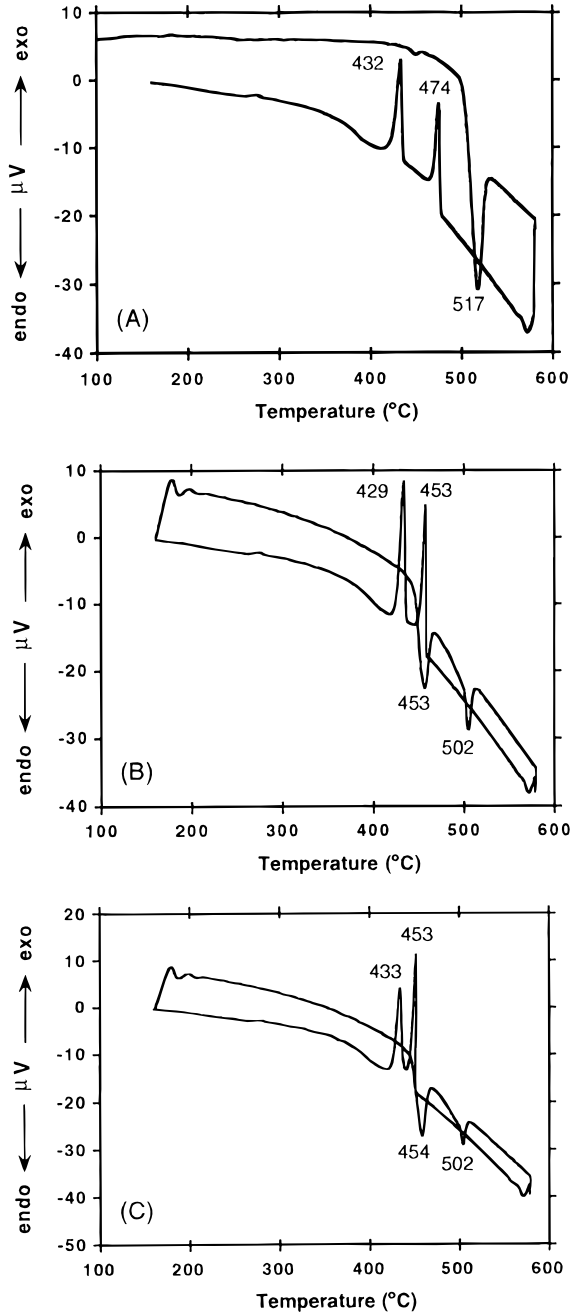

Figure 9. (A) DTA diagram for $K_2Au_2P_2Se_6$ (first cycle). (B) Second DTA cycle of $K_2Au_2P_2Se_6$, showing two phases. (C) Third DTA cycle of $K_2Au_2P_2Se_6$.

Scheme 1

$$3K_2Au^{I}{}_2P_2Se_6 \longrightarrow K_6Au^{I}{}_{1.5}Au^{III}{}_{1.5}(P_2Se_6)_3 + 3Au^{o}$$

teristic for the $[P_2Se_6]^{4-}$ group.[1,4,5,9,12] All compounds **I**−**V** possess weak absorptions below 200 cm^{-1} which probably are due to Au−Se vibrations. The far-IR spectra of **VI**−**VIII** and $AAuP_2S_7$ (**IX**, **X**) are quite complex. Absorptions in the 620−400 cm^{-1} range for **VI**−**VIII** are tentatively assigned to the P−S vibrational stretching modes by analogy with the $AuPS_4$,[11] MPS_4 (M = In, Ga, and Ba),[32] and $KNiPS_4$.[33] Absorptions below 400 cm^{-1} are assigned to S−P−S bending modes and Au−S vibrations.[24] By comparison to $KAuS_5$ the absorption

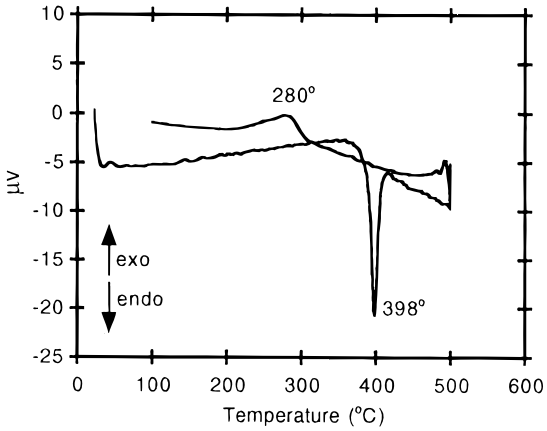

Figure 10. Typical DTA diagram for the $AAuP_2S_7$ (A = K).

at ∼320 cm^{-1} can be tentatively assigned as a Au−S stretching vibration.[34] The $AAuP_2S_7$ shows a number of absorptions in the 600−400 cm^{-1} range. The sharp absorption at 458 cm^{-1} represents the characteristic P−S−P stretching vibration, while the remaining absorptions are due to the $-PS_3$ stretching vibrations by analogy to $Ag_4P_2S_7$.[35,36] Absorptions below 400 cm^{-1} are assigned to Au−S stretching vibrations and P−S deformation modes.

The Raman spectra of **I**−**V** display absorptions in the 224−500 cm^{-1} that are tentatively assigned to P−Se, and the absorptions below 200 cm^{-1} are assigned to Au−Se stretching vibrations. Similarly, the Raman of **VI**−**X** display absorptions in the 217−670 cm^{-1} that are tentatively assigned to P−S and the absorptions below 200 are assigned to Au−S stretching vibrations.

Differential thermal analysis (DTA) data, see Figure 8, followed by careful XRD analysis of the residues, show that **I**−**III** melt congruently, at 442, 483, and 478 °C, respectively. The DTA of **IV** and **V** show a single endothermic peak ∼517 °C, but two exothermic peaks at ∼474 and ∼432 °C appear upon cooling (Figure 9A). On subsequent heating, a second endothermic peak is observed at ∼453 °C (Figure 9B) while the 517 °C endothermic peak shifts to 502 °C and the exothermic peak at 474 °C shifts to 453 °C. Four additional cycles did not alter the position of the peaks, but the relative intensity of the two exothermic peaks was reversed. (In each cycle the sample was isothermed for 2 h at 580 °C.) The last DTA cycle is given in Figure 9C. Examination of the residue by powder XRD revealed that most of the compound had undergone a phase transformation to $K_6Au^{I}{}_{1.5}Au^{III}{}_{1.5}(P_2Se_6)_3$,[12] according to the self-redox reaction of Scheme 1. The latter is a mixed-valence compound that contains both Au^+ and Au^{3+}. This indicates that $A_2Au_2P_2Se_6$ is unstable with respect to disproportionation of the Au^+ oxidation state. Crystals of **VI**, **VII**, and **IX** melt congruently. The DTA of **VIII** indicates that it melts incongruently at 375 °C, converting to another form, β-Cs_2AuPS_4, which is X-ray isomorphous to K_2AuPS_4. The DTA of **X** shows that it too melts incongruently at 404 °C to form a mixture of $RbAuP_2S_7$ and an as yet unknown phase. A typical thermogram for **IX** is shown in Figure 10. Table 13 summarizes the optical and melting point data for all compounds.

The structural diversity displayed in chalcophosphate flux grown compounds is astonishing and is due mainly to the variety

(32) (a) D'ordyai, V. S.; Galagovets, I. V.; Peresh, E. Yu.; Voroshilov, Yu. V.; Gerasimenko, V. S.; Slivka, V. Yu. *Russ. J. Inorg. Chem.* **1979**, *24*, 1603−1606.
(33) Sourisseau, C.; Cavagant, R.; Fouassier, M.; Brec, R.; Elder, S. H. *Chem. Phys.* **1995**, *195*, 351−369.
(34) Park, Y. Ph.D. Dissertation, Michigan State University, E. Lansing, MI, 1991.
(35) Menzel, F.; Ohse, L.; Bröckner, W. *Heteroatom Chem.* **1990**, *1*, 357−360.
(36) (a) Queigrec, M.; Evain, M.; Brec, R.; Sourisseau, C. *J. Solid State Chem.* **1992**, *189*, 209−215.

of possible $[P_yQ_z]^{n-}$ groups and the large diversity of binding modes of each $[P_yQ_z]^{n-}$ group. The fluxes provide a convenient entry into the hitherto unknown Au chemistry, and preliminary results indicate that the elusive ternary Au/P/Q (Q = S, Se) compounds can also be synthesized and structurally characterized.[37] At a constant temperature, control of flux composition and basicity is key in controlling which $[P_yQ_z]^{n-}$ ligands will appear in the compounds. This enables some degree of control on the reaction outcome, in the sense that one can construct structures with preselected ligands. The final structure type is still difficult to predict. Finally, there are significant chemical differences between thiophosphate and selenophosphate chemistry, and so both types of species should be explored to better comprehend this interesting area of chemistry.

(37) Chondroudis, K.; Hanko, J. A.; Kanatzidis, M. G. Work in progress.

Acknowledgment. Financial support from the National Science Foundation DMR-9527347 is gratefully acknowledged. M.G.K. is an A. P. Sloan Foundation Grant Fellow and a Camille and Henry Dreyfus Teacher Scholar (1993−98). This work made use of the SEM facilities of the Center for Electron Optics at Michigan State University.

Supporting Information Available: Tables of X-ray parameters, fractional atomic coordinates of all atoms, anisotropic and isotropic thermal parameters of all atoms, interatomic distances and angles, and calculated and observed X-ray powder patterns for **I**, **IV**, **VI**, **VIII**, and **IX** (39 pages). Ordering information is given on any current masthead page.

IC961376+